

DNS of a Backward-Facing Step at high Reynolds number. Towards a better understanding of RANS-LES transition in DES models.

A. Pont-Vílchez*, F.X. Trias* and A. Oliva*
Corresponding author: arnau@cttc.upc.edu

* Heat and Mass Transfer Technological Center (CTTC)
Universitat Politècnica de Catalunya-BarcelonaTech (UPC)
ESEIAAT, Colom 11, E-08222 Terrassa, Barcelona, Spain.

Abstract: A DNS of an incompressible fluid flow over a Backward Facing Step (*BFS*) with an Expansion Ratio (*ER*) equal to 2, $ER = H/(H - h)$, has been performed. Where h and H represent the step and the outlet heights, respectively. A turbulent channel flow at $Re_\tau = 395$ has been used as an inflow. The DNS data has been compared with the results obtained by a DDES-SA turbulence model, to assess the non-zonal model accuracy. Particular attention has been paid to the *Grey Area* (*GA*), where the effects of the temporal scheme have been analysed considering simplified tests (without turbulence model, i.e. *coarse-DNS*). This study intends to shed light on the strong damping suffered by the resolved turbulence, which is severely affected by the *Courant* number (*Co*) and the time integration scheme. Moreover, the suitability of the implicit schemes in comparison of the explicit ones is also questioned, as $Co < 1$ are commonly typical in Hybrid RANS-LES simulations. Although the DDES-SA is the unique Hybrid model treated in this paper, the conclusions extracted from this study could also be applied to other Hybrid turbulence models.

Keywords: Direct Numerical Simulation, Turbulence Modeling, Detached Eddy Simulation.

1 Introduction

Direct Numerical Simulations (DNSs) are considered a powerful tool for studying complex flow phenomena, solving problems that current turbulence models are incapable to deal with. Despite its industrial applicability is very limited because of its expensive cost, this technique can be really worthy for testing the existing models' performance. In particular, those which solve the flow unsteadiness, such as LES and Hybrid RANS-LES. The complex multiscale flows assessed by these models are commonly validated through experimental studies. Although this step is an important requirement for any turbulence model, in contrast to DNSs, experimental data is usually quite limited due to measurement constraints. In this context, DNS is presented as a suitable tool for extending the experimental validation process, allowing full control of the studied flow and providing high-quality data that could be challenging, even impossible, to obtain through empirical analysis.

Amongst the abovementioned turbulence models, Hybrid RANS-LES have been gaining importance during the last decades. The incapability of RANS models for predicting complex flow behaviour (separated flows, reattachments, adverse pressure gradient...), the need of transient data for assessing time-dependent phenomena (Computational Aeroacoustics, Fluid-Structure Interaction...) and the increasing affordability of computational resources during the last half century are the main causes. In this regard, Detached Eddy Simulation (DES) [1] family models have become popular because of their user-friendly non-zonal approach and their proved success in several flow configurations in contrast to other techniques (such as RANS). Even

though important improvements [2, 3] have been achieved, DES models still suffer from certain shortcomings, which are well-known since their origin [1]. Some of them have already been fixed [2], whereas some other still remain, such as the delay from RANS to LES into the transition zone, also known as the *GA*. This delay severely affects the shear layer development, even triggering wrong behaviours downstream of the transition. So far, different approaches have been proposed in order to mitigate the *GA*; e.g. the recent compendium of the newest *Grey Area Mitigation* (*GAM*) techniques carried out by published by Mockett et al. [4]. Regarding the DNS benefits, all proposals presented in this work [4] have been validated through DNS, as far as possible. Only complex flows have been tested through experimental results due to the lack of DNS data.

In this context, a DNS of an incompressible fluid flow over a *BFS* with an *ER* equal to 2 has been performed, using a turbulent channel flow at $Re_\tau = 395$ as an inflow. DNS and DDES-SA turbulence model results have been compared to assess the non-zonal model accuracy. Particular attention has been paid to the *GA* phenomenon, where the possible effects of the time integration techniques have been studied through simplified tests (without turbulence model, i.e. *coarse-DNS*). This study intends to shed light on the strong damping suffered by the resolved turbulence, which is severely affected by the *Courant* number (*Co*) and the time integration scheme. Moreover, the suitability of the implicit schemes in comparison of the explicit ones is also questioned, as Hybrid RANS-LES simulations require $Co < 1$.

Even though the *BFS* case is not especially challenging due to the sudden geometrical expansion, it is a suitable case for studying the *GA*; considering that Kelvin-Helmholtz (*KH*) instabilities should arise just after the sharp step-edge. Other situations with induced adverse pressure gradient separation are definitely more challenging, but in this case, the *GA* and the predictive capability of the RANS phenomena would be coupled. This coupling makes this kind of cases unsuitable for distinguishing the effect of the different *GAM* techniques.

The rest of the paper is arranged as follows. In the next section, the governing equations and the problem definition are described together with an overview of the numerical methods for the DNS and the DDES turbulence model. The core of the results is in Section 3, where the main features of the time-averaged flow are discussed on the basis of a direct comparison with DNS, DDES and previous experimental results obtained by Ötügen [5] and Nadge et al.[6]. Moreover the effects of different time integration techniques into the *GA* phenomenon has been also been studied, through simple tests (without turbulence model, *coarse-DNS*). Finally, relevant results are summarized and conclusions are given in the last section.

2 Governing Equations and numerical methods

First, a schema of the problem under consideration is shown in Figure 1. The dimensions of the *BFS* are $38h \times 2h \times Nh$ in the stream-wise, cross-stream and span-wise direction, respectively, where N depends on the studied case. The sudden expansion is located at $L_u = 6h$ from the inflow, whereas the domain length downstream of the step is $L_d = 32h$. The origin of coordinates is placed at the sharp edge.

2.1 DNS ($N = 2\pi$)

The DNS configuration is briefly described in the following subsection. For further information, we refer the reader to the original DNS paper [7]. The incompressible Navier-Stokes (NS) equations in primitive variables are considered

$$\partial_t u_i + u_j \partial_j u_i = -\partial_i p + \nu \partial_j^2 u_i; \quad \partial_i u_i = 0, \quad (1)$$

where u_i is the velocity field, p represents the kinematic pressure, and ν is the kinematic viscosity.

The incompressible NS equations are discretised on a non-uniform structured staggered mesh, and a fully 4th-order symmetry-preserving discretisation [8] scheme is used. For the temporal discretisation, a 2nd-order fully explicit one-leg scheme is used for both the convective and diffusive terms [9]. The classical fractional step projection method [10] is used for coupling the velocity-pressure system. In regard to the boundary conditions, a turbulent unsteady channel flow at $Re_\tau = 395$ is imposed at the inflow [11]. A convective boundary condition is used at the outflow. Finally, periodic boundary conditions are imposed in the span-wise direction, whereas the walls are considered no-slip.

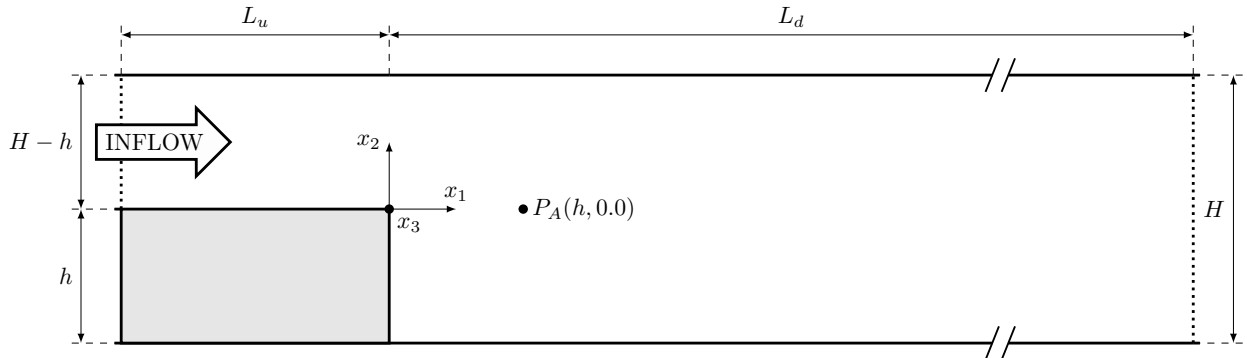


Figure 1: Schematic figure of the Backward Facing Step problem, $ER = H/(H - h) = 2$, and details about its geometry and grid spacing (size of zones and concentration factors; arrows indicate the grid refinement direction). Not to scale.

A Cartesian staggered mesh with $1510 \times 302 \times 360 \sim 165e^+6$ grid points has been used to cover the computational domain in the stream-wise, cross-stream and span-wise direction, respectively. The grid spacing in the periodic x_3 -direction is uniform, whereas the rest of directions use piece-wise hyperbolic-tangent functions. The linear stability of the time-integration scheme has been adapted to the instantaneous flow conditions in order to use the maximum time-step ($\Delta t \sim 1.57e^{-4}h/u_\tau$) possible, where u_τ refers to the skin friction velocity at the inflow. Regarding the verification of the code, the reader is referred, for example, to Trias et al.[12].

2.2 DDES ($N = 2$)

The DDES turbulence model presented by Spalart et al.[2] has been used in this paper, including the Ψ term specially designed to override the unintended low- Re terms. In this case, all DDES simulations have been run using *OpenFOAM*.

The Hybrid convection scheme presented by Travin et al. [13] for hybrid *RANS/LES* calculations is used in this simulation. For the temporal discretisation, a 2^{nd} -order implicit *backward* scheme is considered. The velocity-pressure system is coupled using the well-known PISO algorithm. Concerning the boundary conditions, the same ones applied in DNS have also been used in DDES, but considering a steady turbulent channel flow inflow instead. The inflow data has been obtained through a previous turbulent channel flow simulation using the Spalart-Allmaras (*SA*) model. The eddy-viscosity transported by the *SA* model, $\hat{\nu}$, has also been obtained from the channel flow simulation at the inflow, whereas a Neumann condition has been applied at the outflow. Finally, the $\hat{\nu}$ is set to zero at walls, while the boundaries in the span-wise direction remain periodic.

In contrast to the DNS case, a body-fitted collocated mesh has been used containing $\sim 1.3e^+6$ grid points. The grid spacing in the periodic x_3 -direction is uniform, whereas the rest of directions are refined close to the walls and in the shear layer zone. The *Courant* value has remained constant ($Co = 0.80$), leading to an average time-step $\sim 5.76e^{-4}h/u_\tau$, which is higher than the time-step assessed by the DNS.

3 Results and Discussions

Averages over the two statistically invariant transformations (time and x_3 -direction) are carried out for all the fields denoted by $\langle \cdot \rangle$.

3.1 Comparison DNS vs DDES-SA results

A set of comparisons between the DNS and the DDES results is presented in this section. First of all, the mean flow in the stream-wise direction obtained by DNS and DDES-SA is presented in Fig 2. A non-negligible misalignment is observed just downstream of the flow, where the *GA* effects become relevant ($0 < x_1 < 4$).

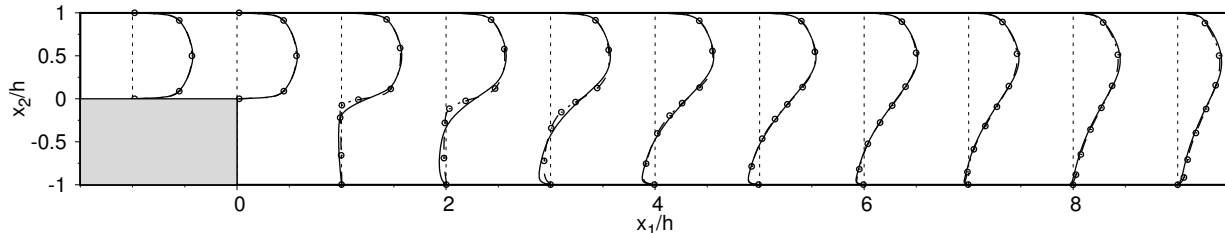


Figure 2: Mean velocity in the stream-wise direction along the recirculation region. Where DNS results are indicated by solid lines (—) and the DDES-SA data is referred by dashed-dotted lines (- o - ·).

The delay of the shear layer produced by the *GA* leads to a lack of diffusion, allowing the stiff velocity profiles located just after the sudden expansion. However, once the shear layer is developed downstream of the step-edge, the flow profile alignment is recovered ($x_1 \geq 4$).

Apart from their effects into the stream-wise mean velocity, the delay at the shear layer produced by *GA* can be better appreciated in Fig. 3, where the resolved Reynolds stresses are shown. Even though flow instabilities would be expected just downstream of the step-edge (as the Hybrid model switch from RANS to LES), a severe delay of the Reynolds stresses is present ($x_1 \approx 1$).

An absence of Reynolds stresses is also observed upstream of the step-edge and downstream at the upper wall region. In this case, both behaviours are expected as the Hybrid model works as a pure Spalart-Allmaras (*SA*) in these regions. That is true except for the oscillations in the stream-wise direction at the upper wall (Fig. 3, top), which are recovered due to an undesired interaction between the RANS and LES zones. In fact, it is another kind of *GA* effect, but in this case the LES region disturbs the RANS one, e.g. where the small kinematic eddy viscosity values, ν_t , located at the LES region are convected to the upper wall, producing a depletion of the ν_t in the RANS region. This reduction can be easily observed in Fig.4, where the ratio ν_t/ν of a DDES-SA simulation is compared with a RANS-SA one. Apart from the premature depletion of the ν_t/ν at the upper wall, the deliberate reduction of this parameter into the LES region can also be observed ($x_1 > 8$).

In particular, the ν_t reduction at the upper wall leads to an abrupt recovering of the skin friction, $\langle C_f \rangle$, which can be well observed in Fig. 5 (left-D). In contrast to the DNS and the other RANS models, there is a lack of recovery region in the DDES-SA simulation, achieving a “channel flow like” behaviour just after the flow separation. Besides the unfortunate $\langle C_f \rangle$ behaviour at the upper wall, it is worth noting here the flow separation resilience shown by the DDES-SA model in Fig. 5 (left- C and right) respect to the other RANS models. Moreover, the over-prediction of the $\langle C_f \rangle$ peak at the lower wall is considerably mitigated in the DDES-SA (left-B), and a surprisingly good agreement with the DNS data is also observed. However, the *GA* phenomenon downstream of the step-edge contributes to a strong relaminarization at the very beginning of the recirculation bubble (left-A).

3.2 Time integration sensitivity

The incapability of the DDES-SA model for triggering flow instabilities at the shear layer ($x_1 \approx 1$) indicates that some *GAM* techniques should be applied. In this regard, Mockett et al. [4] recently published a detailed and comprehensive compendium of the newest *GAM* techniques. In essence, all methods try to trigger the transition of the shear layer, using different approaches; e.g. some of them decrease the ν_t , while the other tries to apply stochastic forces to achieve the same purpose. It is worth noting here that the latter strategy could be more suitable in this case, as the DNS inflow carries strong oscillations, which are not present at the steady turbulent DDES-SA inlet. Therefore, we should not expect higher oscillations than the DNS case at the shear layer.

However, irrespective of the chosen *GAM* methodology, it is clear that at the LES zone we would not expect any extra dissipation source (contributing to the oscillations reduction) besides those provided by the natural effects, the turbulent model and the mesh resolution. In particular, we are referring to the numerical (and artificial) dissipation produced by the numerical schemes (spatial and temporal). We understand that sometimes it may be useful, as it provides extra stability, but it is also artificial and usually out of

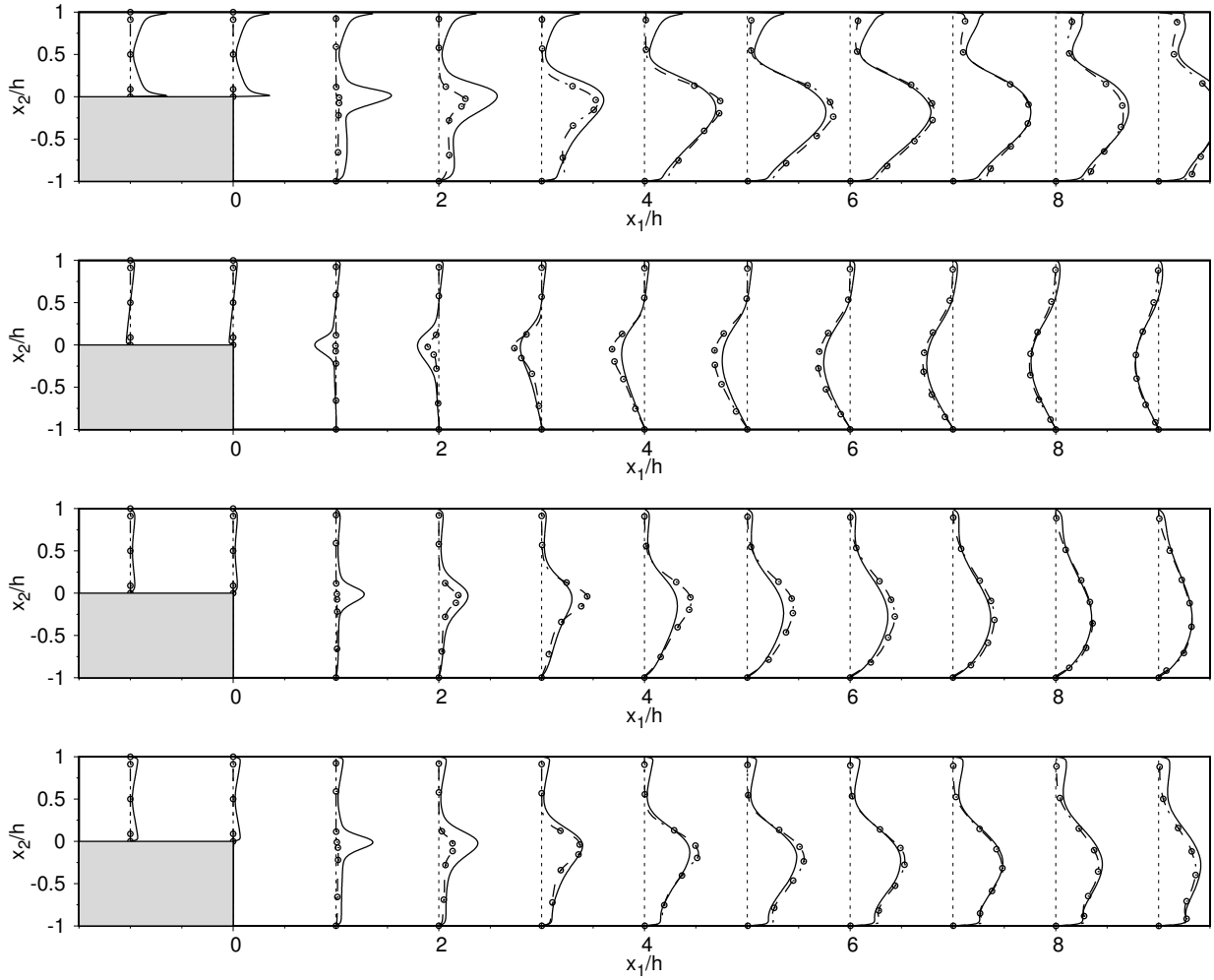


Figure 3: Resolved Reynolds stresses in the stream-wise ($\langle u_1' u_1' \rangle$, top), crossed ($\langle u_1' u_2' \rangle$, middle-top), normal ($\langle u_2' u_2' \rangle$, middle-bottom) and spanwise ($\langle u_3' u_3' \rangle$, bottom) directions along the recirculation region. Where DNS results are indicated by solid lines (—) and the DDES-SA data is referred by dashed-dotted lines (- o - ·).

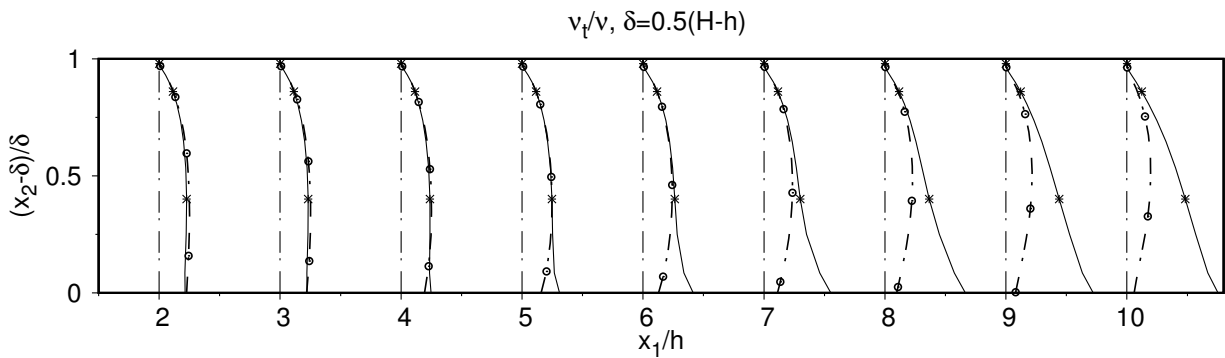


Figure 4: Comparison of the kinematic eddy viscosity vs the kinematic natural viscosity ratio, ν_t/ν , of the DDES-SA. Where DDES-SA data is referred by dashed-dotted lines (- o - ·) and RANS-SA is denoted as (*—).

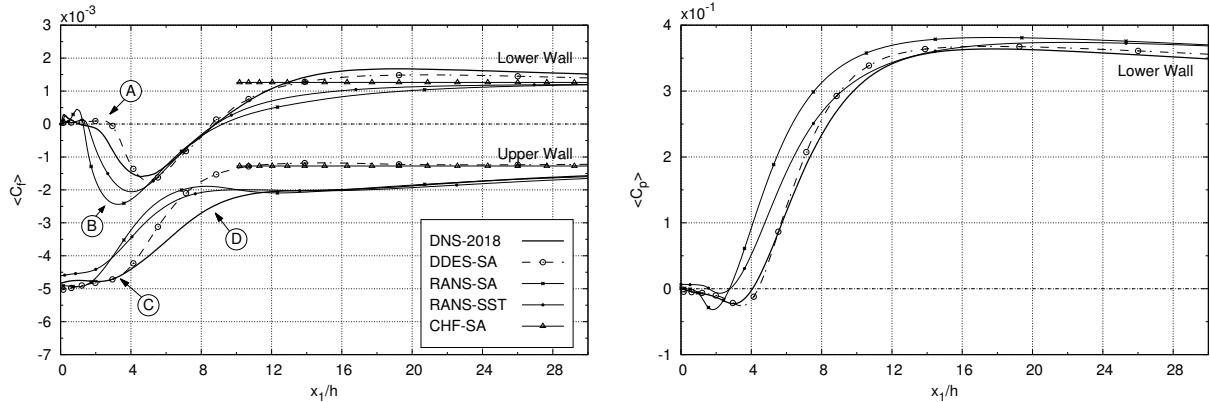


Figure 5: Comparison of the skin friction (left), $\langle C_f \rangle$, and the pressure coefficient (right), $\langle C_p \rangle$ at $Re_\tau = 395$ of the DNS data with the DDES-SA, the RANS-SA and the RANS-SST results. The $\langle C_f \rangle$ of a channel flow with the BFS outflow geometry is also displayed (CHF-SA).

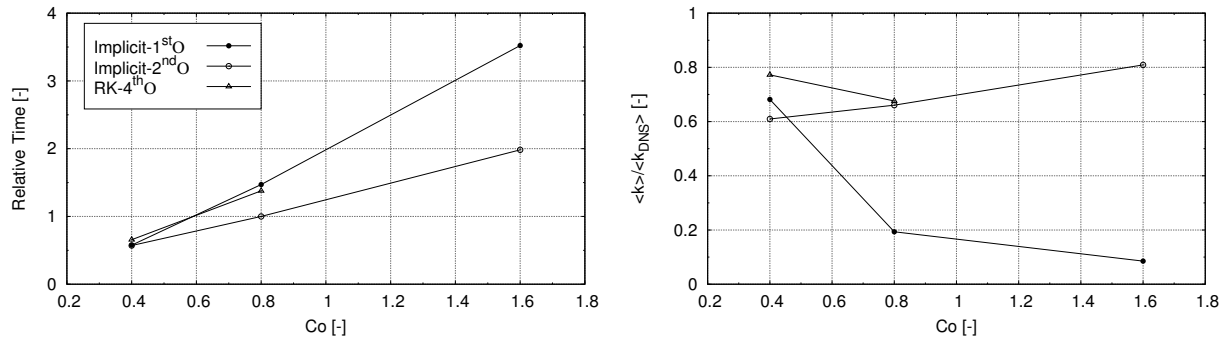


Figure 6: The computational cost (left) of different time integration schemes, including their time step sensitivity, Co . The turbulent kinetic energy (right) at the point P_A (Fig.1) resolved by the *coarse-DNS* respect to the the DNS $\langle k_{DNS} \rangle$. The computational cost is relative to the *Implicit 2nd-order* and $Co = 0.8$, which is set to 1.

control. Concerning the numerical dissipation produced by the spatial scheme at the LES zone, it can be easily fixed using a symmetry-preserving scheme. In contrast, the extra dissipation provided by the Time Integration Scheme is not that clear. For instance, DES literature is full of works recommending a $Co < 1$ [14], provided that an acceptable behaviour of the flow instabilities at the shear layer is desired. Hence, in this work, special attention has been paid in the time step sensitivity, as well as how it affects different time integration schemes. These are: *Implicit 1st-order* (Euler), *Implicit 2nd-order* (Backward, subsec. 2.2) and the explicit low-dissipative *RK 4th-order* (Runge-Kutta) [15]. The latter has been chosen in order to analyse the capability of the explicit schemes in comparison to the implicit ones, taking advantage the Co usual recommendation ($Co < 1$). The *Courant* number related to the viscous terms, Co_ν , has also been computed in the *BFS* case, resulting in the same order of magnitude that the convective one, Co . However, in cases where the Co_ν was higher than Co , explicit schemes would be discouraged.

Due to the lack of *GAM* adapted into the code, as a first approach the study has been carried with *coarse-DNS*, instead of using DDES-SA. Otherwise, the *GA* would inhibit any possible oscillation at the shear layer ($x_1 = 1$). In order to avoid any possible instability coming from the inflow ($x_1 = -L_u$), this part of the domain has been removed, so the turbulent steady profile goes directly into the sudden expansion. Apart from that, the mesh and boundary conditions presented at section 2.2 are conserved.

The results presented in Fig. 6 shows the influence of using different time integration schemes, as well as their strong and varied time step sensitivity (Co). Apart from that, before explaining each numerical scheme

trend, it would be nothing here that the $\langle k_{DNS} \rangle$ is only a reference of the flow fluctuations at this position, which would never be reached in this case configuration (because of the reasons explained above).

- Implicit 1st-order

It exhibits a strong decrease of the resolved turbulence along the Co , which is attributed to its intrinsic numerical dissipation [16]. Therefore, this is a case where the $Co < 1$ recommendation in DDES models fits well with the observed trend, at the expense of the computational cost, Fig. 6(left). The low resources needed by $Co \geq 0.8$ are due to the lack of turbulence present in the shear layer, so it could be considered that the results are not acceptable. Hence, in this case, a *GAM* based on reducing the ν_t would not be able to trigger any turbulence at the shear layer if a $Co \geq 0.8$ is used.

- Implicit 2nd-order

This is a well-known numerical scheme in the DES community, which was also used when the time step sensitivity was firstly notified [14], and also in recent research on *GAM* techniques [17]. The results present in Fig. 6 (right) are quite surprising, as they apparently clash with the $Co < 1$ recommendation. However, the positive slope could be justified due to a lack of numerical dissipation and a possible back-scattering effect, which would be triggered because of the incapability of the time step to reproduce the smallest scales. In any case, it is clear that further research on this topic is needed. On the other hand, the computational resources are higher than the other when $Co \leq 0.8$, whereas the opposite is true when $Co > 0.8$. Therefore, its suitability is restricted to $Co > 0.8$, but at the same time, it clashes with the $Co < 1$ recommendation.

- RK 4th-order [15]

This temporal scheme has been chosen to analyse the capability of the explicit schemes in comparison to the implicit ones, taking advantage of the Co usual recommendation ($Co < 1$). Apart from presenting the lowest computational resources (left) at the recommended area ($Co \leq 1$), the levels of turbulence are also quite high at $Co \geq 0.8$ (right), in comparison to the explicit ones. However, it remains to be seen if this computational advantage is going to be sustained in a DDES simulation, where extra transport equations for the turbulence models are also solved.

3.3 Explicit RK 4th-order in DDES-SA

The capabilities of different time integration schemes have been assessed in the last subsection. The advantages offered by the RK 4th-order in the *coarse-DNS* simulations have been rather encouraging, so its performance in DDES-SA has been also studied. In particular, the resolved Reynolds stresses in the stream-wise direction, $\langle u'_1 u'_1 \rangle$, have been compared in Fig.7. As it was expected, the well-known delay at the shear layer remains in the DDES-SA simulations (**B**), either by the *Implicit 2nd-order* (left) and the *RK 4th-order* (right), in comparison to the *coarse-DNS* (bottom). It is also worth noting that there is an absence of turbulence at the entrance in all cases (**A**). On the other hand, the *coarse-DNS* suffers an increase in the flow oscillations at the upper wall (bottom-**C**) vs the DDES-SA simulations (top). They are mainly triggered by a non-physical recirculation bubble, which is caused by the lack of mesh resolution. Therefore, it can be noticed that only small differences are observed between the DDES-SA, concluding that the influence of using different integration schemes is not that high. In addition, the computational cost is significantly lower in the explicit case ($\sim 10\%$). Even though a considerable reduction with the *RK 4th-order* vs the *Implicit 2nd-order* is maintained, it is not as high as the $\sim 30\%$ observed in Fig.6 (top). This trend is rather surprising, as in theory, the gap in the computational resources should be intensified (instead of reduced) in the DDES-SA, due to the additional transport equation it contains. However, those results are quite promising, not only because of the cost reduction, but also the implementation simplicity offered by the explicit schemes vs the implicit ones. Finally, a similar analysis considering the *GAM* is going to be studied in further work, once they are implemented.

4 Conclusions and Future Work

The recent DNS data of a BFS at $Re_\tau = 395$ and $ER = 2$ has been compared with the DDES-SA, a hybrid turbulence model. Their differences have been discussed, and particular attention has been paid to the rapid

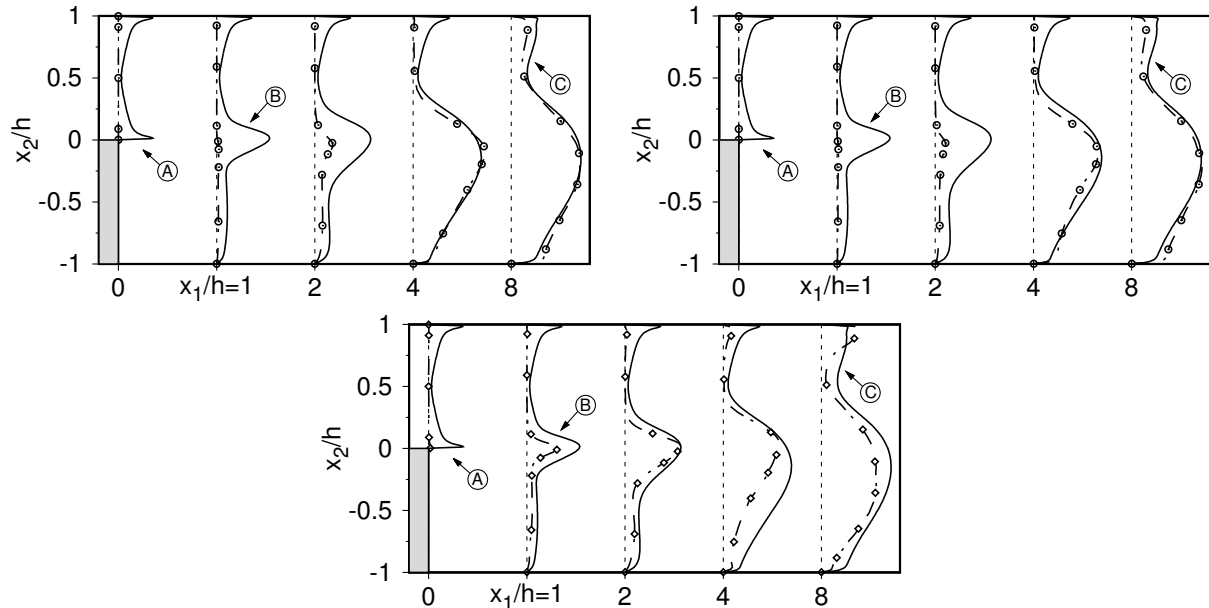


Figure 7: Resolved Reynolds stresses in the stream-wise direction ($\langle u_1' u_1' \rangle$) along the recirculation region, using an *Implicit* 2nd-order (left) and a *RK* 4th-order (right,bottom) with $Co \sim 0.8$. Where DDES results (top) are indicated by dashed-dotted-circled lines (- o - ·) and the *coarse-DNS* (bottom) data is referred by dashed-dotted lines (- ◊ - ·). DNS results are represented by solid lines (—) in both graphs.

skin friction recovery at the upper wall, as well as the lack of instabilities due to the *GA* phenomenon. The former has been attributed to the strong intrusion of the LES region into the RANS one, drastically reducing the nu_t at the upper wall and therefore the $\langle C_f \rangle$. On the other hand, instead of studying the newest *GAM* techniques, the effect of the time step and the time integration schemes into the shear layer instabilities has been considered. In this analysis, the unsuitability of the *Implicit* 1st-order due to its strong dissipation has been shown. Moreover, the well-known recommendation of using $Co < 1$ in DES simulations has been questioned due to the surprising results observed in the *Implicit* 2nd-order scheme, where further work is going to be needed. Apart from that, the explicit scheme (*RK* 4th-order) have also been considered, showing the best performance either by the level of resolved turbulence or the computational resources. Finally, the influence of the *RK* 4th-order in a DDES-SA simulation has also been compared with the *Implicit* 2nd-order, in order to assess its behaviour. Similar results have been obtained, indicating the suitability of the explicit scheme in the DDES-SA. However, further research will be also needed for studying the explicit time scheme behaviour, once the *GAM* techniques are implemented.

Acknowledgements

This work has been financially supported by the *Ministerio de Economía y Competitividad*, Spain (No. ENE2017-88697-R). A.P.V. is supported by a *FI-DGR 2016* predoctoral contract (No. 2018FI_B2_00072) financed by *Generalitat de Catalunya*, Spain. F.X.T. is supported by a *Ramón y Cajal* postdoctoral Contract (No. RYC-2012-11996) financed by the *Ministerio de Economía y Competitividad*, Spain. The authors thankfully acknowledges the the collaboration with Dr. Revell A. at the University of Manchester, as well as the computer resources at MareNostrum and the technical support provided by the Barcelona Supercomputing Centre (RES-FI-2017-2-0041).

References

- [1] P. R. Spalart, W.-H. Jou, M. Strelets, and S. Allmaras, “Comments on the Feasibility of LES for Wings, and on a Hybrid RANS/LES Approach,” 1997.

- [2] P. R. Spalart, S. Deck, M. L. Shur, K. D. Squires, M. K. Strelets, and A. Travin, “A new version of detached-eddy simulation, resistant to ambiguous grid densities,” *Theoretical and Computational Fluid Dynamics*, vol. 20, no. 3, pp. 181–195, 2006.
- [3] M. L. Shur, P. R. Spalart, M. K. Strelets, and A. K. Travin, “A hybrid RANS-LES approach with delayed-DES and wall-modelled LES capabilities,” *International Journal of Heat and Fluid Flow*, vol. 29, no. 6, pp. 1638–1649, 2008.
- [4] C. Mockett, M. Fuchs, F. Thiele, S. Wallin, S. H. Peng, S. Deck, J. C. Kok, H. V. D. Ven, A. Garbaruk, M. Shur, M. Strelets, A. Travin, H. van der Ven, A. Garbaruk, M. Shur, M. Strelets, and A. Travin, “Non-zonal approaches for grey area mitigation,” in *Notes on Numerical Fluid Mechanics and Multidisciplinary Design*, 2018, vol. 134, pp. 17–50. [Online]. Available: <http://link.springer.com/10.1007/978-3-319-52995-0>
- [5] M. Ötügen, “Expansion ratio effects on the separated shear layer and reattachment downstream of a backward-facing step,” *Experiments in Fluids*, vol. 10, no. 5, 1991.
- [6] P. M. Nadge and R. N. Govardhan, “High Reynolds number flow over a backward-facing step: Structure of the mean separation bubble,” *Experiments in Fluids*, vol. 55, no. 1, 2014.
- [7] A. Pont-Vilchez, F. X. Trias, A. Gorobets, and A. Oliva, “Direct Numerical Simulation of Backward-Facing Step flow at $Re_{\tau}=395$ and expansion ratio 2,” *Under Review to the Journal of Fluid Mechanics*.
- [8] R.W.C.P.Verstappen and A.E.P.Veldman, “Symmetry-Preserving Discretization of Turbulent Flow,” *Journal of Computational Physics*, vol. 187, pp. 343–368, 2003.
- [9] F. Trias and O. Lehmkuhl, “A self-adaptive strategy for the time-integration of Navier-Stokes equations,” *Numerical Heat Transfer, part B*, vol. 60, no. 2, pp. 116–134, 2011.
- [10] A.J.Chorin, “Numerical Solution of the Navier-Stokes Equations,” *Mathematics of Computation*, vol. 22, pp. 745–762, 1968.
- [11] A. Meri and H. Wengle, “DNS and LES of turbulent backward-facing step flow using 2nd-and 4th-order discretization,” *Advances in LES of Complex Flows*, pp. 99–114, 2002. [Online]. Available: <http://www.springerlink.com/index/N4745881XR53630K.pdf>
- [12] F.X.Trias, M.Soria, A.Oliva, and C.D.Pérez-Segarra, “Direct numerical simulations of two- and three-dimensional turbulent natural convection flows in a differentially heated cavity of aspect ratio 4,” *Journal of Fluid Mechanics*, vol. 586, pp. 259–293, 2007.
- [13] P. Spalart, M. Shur, M. Strelets, and A. Travin, “Sensitivity of Landing-Gear Noise Predictions by Large-Eddy Simulation to Numerics and Resolution,” *50th AIAA Aerospace Sciences Meeting including the New Horizons Forum and Aerospace Exposition*, no. January, pp. 1–20, 2012.
- [14] C. Mockett, “A comprehensive study of detached-eddy simulation,” *PhD Thesis: TU Berlin*, 2009.
- [15] V. Vuorinen, J. Keskinen, C. Duwig, and B. J. Boersma, “On the implementation of low-dissipative Runge-Kutta projection methods for time dependent flows using OpenFOAM®,” *Computers and Fluids*, vol. 93, pp. 153–163, 2014.
- [16] V. D. Alessandro, L. Binci, S. Montelpare, and R. Ricci, “On the development of OpenFOAM solvers based on explicit and implicit high-order Runge–Kutta schemes for incompressible flows with heat transfer,” *Computer Physics Communications*, vol. 222, pp. 14–30, 2018.
- [17] M. L. Shur, P. R. Spalart, M. K. Strelets, and A. K. Travin, “An Enhanced Version of DES with Rapid Transition from RANS to LES in Separated Flows,” *Flow, Turbulence and Combustion*, vol. 95, no. 4, 2015.